Uptake of Phenylalanine and Tyrosine by a Strong-Acid Cation Exchanger

The equilibrium and rate of uptake of the amino acids phenylalanine and tyrosine by Amberlite 252, a strongly acidic, cation-exchange resin, have been investigated. Uptake of the amino acids by the hydrogen form of the resin occurs primarily by the stoichiometric exchange of hydrogen ions and amino acid cations. The amount of amino acid taken up by the resin can be calculated as a function of solution pH and amino acid concentration from a model that takes into account both solution and ion-exchange equilibria. The rates of uptake of the two amino acids have been determined experimentally for a closed batch system. The results of experiments in which the resin particle size, the flow rate, and the concentration were varied show that intraparticle transport is dominated by the slow diffusion of amino acid cations through the macroreticular polymer structure of the resin, with some contribution from macropore transport of amino acid cations and zwitterions. An intraparticle diffusion model has been developed to describe these results and predict the performance of fixed-bed operations.

Malcolm S. Saunders, John B. Vierow, Giorgio Carta
Department of Chemical Engineering
University of Virginia
Charlottesville, VA 22901

Introduction

Amino acids have acquired a role of considerable importance in the pharmaceutical, food, and health product industries, as animal feed additives, in medicine, and as intermediates in the chemical industry. Although early technology for the production of amino acids was largely based on recovery from protein hydrolysates, today fermentation with genetically selected bacterial strains constitutes the main production route (Yamada et al., 1972). A number of separation steps are normally taken to recover, separate, and purify the amino acid products from fermentation broths. Typically, cell mass and higher molecular weight proteins are removed first by centrifugation, ultrafiltration, and adsorption onto activated carbon. The products obtained from these operations then undergo various treatments for the removal of salts and amino acid separation. Final purification and recovery in a form suitable for storage and end uses is ultimately obtained by means of chromatographic techniques and by fractional crystallization.

Ion exchange is widely used in various stages of processes for the industrial production of amino acids. Since amino acids exist both as anions and cations, depending upon the pH of the solution in which they are present, ion-exchange materials offer a variety of opportunities for separation and concentration of mixtures of amino acids. Adsorption and desorption from ion-exchange resins may be induced by changing the solution pH. Thus, for example, a cation-exchange resin that has been loaded with an amino acid at a pH at which the amino acid is predominantly in the positively charged form, can easily be regenerated by changing the solution pH to a new value at which the predominant form of the amino acid is negatively charged. The negatively charged form will be eluted rapidly since it is excluded from the resin matrix by the Donnan potential effect. Recovery and concentration of amino acids from dilute solution can be carried out with cation-exchange resins in a cyclic process consisting of a period of operation during which the resin is loaded with amino acid at low pH followed by a period of operation at high pH during which the resin is regenerated using an alkaline solution as a displacer. The resin is then reconverted to its original ionic form with an acid solution. Differences in the values of the ionization constants of various amino acids can be exploited to carry out group separations, for example, acidic amino acids from basic and neutral amino acids. Differences in the specific affinities of amino acids for the resin may be exploited to carry out separations of amino acids with similar ionization constants.

While the use of ion-exchange resins for analytical-scale chromatographic separations of amino acids is well established (Blackburn, 1983), fewer studies have addressed the basic features of equilibrium and mass transfer characteristics of industrial uses of ion-exchange resins for amino acid separations. Hamilton et al. (1960) have analyzed equilibrium and mass

Correspondence concerning this paper should be addressed to Giorgio Carta.

transfer effects in chromatographic columns employed for quantitative analysis of amino acid solutions. Seno and Yamabe (1960, 1961) have examined the equilibrium uptake of a number of amino acids by both cation- and anion-exchange resins in single-component systems. Feitelson (1961, 1963) has carried out studies on the uptake of amino acids at their isoelectric pH by a cation-exchange resin, in the presence of a large excess of buffer. Yu and Wang (1986) and Yu et al. (1987) have addressed the effects of equilibrium on the dynamics of chromatographic columns used for the separation of amino acids and have developed strategies for the optimization of these separations.

In the present study we address a number of aspects of the ion exchange of amino acids in a systematic investigation of the uptake of phenylalanine and tyrosine by a commercial, strong-acid, cation-exchange resin, Amberlite 252. We have obtained measurements of the equilibrium uptake as a function of concentration and pH and have developed methodologies to correlate these results by means of appropriate models. The solution equilibria are modeled using the mass action law for the dissociation reactions of the amino acids together with the condition of electroneutrality. A model for the ion-exchange equilibrium which accounts for the energetic heterogeneity of functional groups in the ion exchanger and for the ionization of amino acids in solution has been found to provide an excellent fit of binary exchange data and an approximate prediction of equilibrium in ternary systems. This basic information can then be incorporated into a general mass transfer model for the prediction of the dynamic behavior of fixed-bed separation processes.

The resin used in this study is macroreticular; that is, it consists of a conglomerate of microspheres made of gel-type resin material. While intraparticle transport in gel-type resins is well understood (Helfferich, 1962; Turner et al., 1966), few studies have been dedicated to porous resins. In these resins intraparticle mass transfer may occur by means of two mechanisms acting in parallel in the radial direction (Patell and Turner, 1980; Yoshida et al., 1985; Yoshida and Kataoka, 1985):

1. Diffusion through the liquid held within the macropores
2. Diffusion through the resin microparticles

The relative importance of the two mechanisms depends upon the relative magnitude of the effective diffusivities in the two phases. In general, as shown by Yoshida and Kataoka (1985), at low solution concentrations mass transfer through the microparticles is dominant, while mass transfer through the macropore liquid is dominant at high solution concentrations. Since in Amberlite 252 (as well as in many similar resins) the microparticles are very much smaller than the resin bead diameter, the diffusion resistance in the radial direction of the microparticles is ordinarily rather small. External mass transfer resistance also affects the rate of uptake. In general, at low solution concentrations external mass transfer resistance is dominant, while intraparticle diffusional resistances are normally dominant at higher solution concentrations (Helfferich, 1962).

No systematic investigation of intraparticle mass transfer in the ion exchange of amino acids appears to have been reported. In this paper, we address the kinetics of the process of uptake of amino acids by the hydrogen form of Amberlite 252 resin in a batch system. Experimental uptake rates are analyzed in terms of models that take into account the resin structure and the complex solution and ion-exchange equilibria that pertain to the amino acid system. The information developed from analyses of the kinetics of the process is then incorporated in a mass transfer model that allows an accurate prediction of breakthrough and elution curves in fixed-bed ion-exchange operations. An effective numerical solution technique based on orthogonal collocation on finite elements has been developed for the solution of the model.

Solution and Ion-Exchange Equilibria

Amino acids are amphoteric molecules with a structure that can be generally represented as $NH_2CHRCOOH$. In aqueous solution the following equilibrium dissociation reactions take place

$$NH_3^+CHRCOOH \rightleftharpoons NH_3^+CHRCOO^- + H^+ \quad (1)$$

$$NH_3^+CHRCOO^- \rightleftharpoons NH_2CHRCOO^- + H^+ \quad (2)$$

For amino acids that have an ionizable R group an additional dissociation reaction should be considered. If the pH and the total concentration of an amino acid, A_i, present in an aqueous solution are known, neglecting the effects of solution nonideality, the concentration of positively charged amino acid may be calculated from

$$C_{A_i^+} = C_{A_i} \Big/ \left(1 + \frac{K_1}{C_{H^+}} + \frac{K_1K_2}{C_{H^+}^2}\right) \quad (3)$$

where K_1 and K_2 are the dissociation constants of the amino acid, C_{A_i} is the total concentration of amino acid, and C_{H^+} the concentration of hydrogen ion. Conversely, if the concentrations of the amino acids A_i present in a salt solution (containing for example NaCl) are known, the solution pH may be calculated from the electroneutrality condition that can be expressed as follows

$$\sum_i C_{A_i^+} + C_{Na^+} + C_{H^+} = \sum_i C_{A_i^-} + C_{Cl^-} + C_{OH^-} \quad (4)$$

where the $C_{A_i^-}$'s are the concentrations of amino acid A_i present in negatively charged form, which are given by

$$C_{A_i^-} = C_{A_i} \Big/ \left(1 + \frac{C_{H^+}}{K_2} + \frac{C_{H^+}^2}{K_1K_2}\right) \quad (5)$$

C_{OH^-} is the concentration of hydroxyl ion, which is given by the dissociation product of water. In general a trial and error solution of Eq. 4 is required to obtain the solution pH and compute $C_{A_i^+}$, when all the C_{A_i} values are given. Once the pH is obtained, the concentrations of positively charged amino acid can be obtained from Eq. 3.

If a single amino acid, A, is present in solution with concentration C_A, Eq. 4 can be solved analytically in the two limiting cases of low pH and high pH values. At low pH values (well below the isoelectric pH), C_{A^-} and, for all but the basic amino acids, C_{OH^-} are negligible. In this case Eqs. 3 and 4 yield

$$C_{A^+} = \tfrac{1}{2}[(C_A + C_0 + K_1) - \sqrt{(C_A + C_0 + K_1)^2 - 4C_AC_0}] \quad (6)$$

and

$$C_{H^+} = \frac{K_1}{C_A/C_{A^+} - 1} \tag{7}$$

where $C_0 = C_{Cl^-} - C_{Na^+}$. At pH values significantly higher than the isoelectric pH, C_{A^+} is essentially zero and no ion exchange with a cation resin will occur. Near the isoelectric pH, Eq. 4 needs to be solved exactly. This can be done numerically using various algorithms. As an example, Figure 1 shows the calculated ionic fraction of amino acid cations, X_A, and the pH of aqueous solutions of phenylalanine, based upon Eqs. 3, 4, and 5. The ionic fraction X_A is defined by

$$X_A = \frac{C_{A^+}}{C_{A^+} + C_{Na^+} + C_{H^+}} \tag{8}$$

As seen in Figure 1, when the value of C_0 is very small or zero, as the total concentration of amino acid in solution is increased the solution pH rapidly approaches the isoelectric pH of the amino acid. Conversely, when the value of C_0 is very large, the amino acid concentration has only a small effect on the solution pH, and the ionic fraction of phenylalanine increases in a nearly linear manner with C_A.

The exchange of an amino acid cation for hydrogen ion on a cation-exchange resin may be described by the following stoichiometric relationship

$$R'H + NH_3{}^+CHRCOOH \rightleftharpoons R'NH_3CHRCOOH + H^+ \tag{9}$$

where R' represents the negatively charged functional groups on the resin. The effect of the concentration of hydrogen ion in solution on the uptake of an amino acid by a cation exchange resin in the hydrogen form is apparent from Eqs. 1, 2, and 9. At low pH the amino acid is largely in its protonated form and is taken up by the resin by ion exchange with H^+. At very low pH values, however, hydrogen ions in solution compete effectively with the amino acid cations and reaction 9 is shifted to the left. Finally, at high pH values the amino acid becomes negatively charged

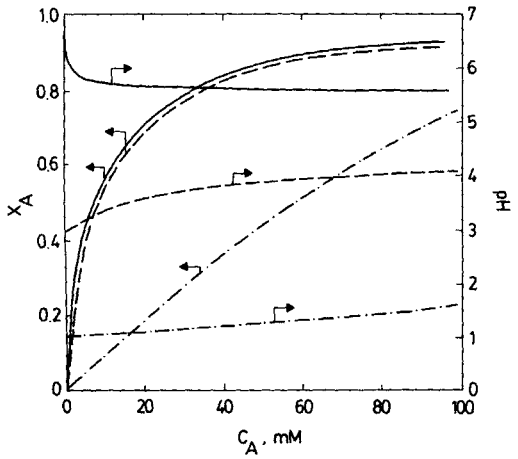

Figure 1. Calculated effects of solution concentration of Phe on ionic fraction of amino acid cations and solution pH.

— $C_0 = 0$; --- $C_0 = 0.001$ mol/L; ···· $C_0 = 0.1$ mol/L.

Table 1. Properties of Amberlite 252

Ion-exchange capacity	5.0 ± 0.2 mmol/g dry resin
Resin density	0.59 ± 0.02 g dry resin/cm^3
Water content	1.16 ± 0.06 g H_2O/g dry resin
Resin porosity	0.24 ± 0.04
Swelling (Na → H)	5%
DVB cross-linking	12%
Avg. particle dia.	0.8 mm

and is excluded from the resin by the Donnan potential effect.

If a third counterion, say Na^+, is present, the exchange of Na^+ and H^+ should be considered according to

$$R'H + Na^+ \rightleftharpoons R'Na + H^+ \tag{10}$$

An additional equation describing the exchange of amino acid cations for sodium ions could also be written, but this, of course, would not be independent of Eqs. 9 and 10.

The occurrence of nonionic adsorption resulting from hydrophobic interactions of the organic side chain of the amino acids with the resin matrix should also be considered, especially with polystyrene-based resins and aromatic amino acids. This effect, if occurring, would result in an uptake capacity that may exceed the total ion-exchange capacity of the resin. Furthermore, the uptake of amino acid by the resin in this case would not be dependent solely upon the concentration of protonated amino acid but, presumably, also upon the concentration of dipolar amino acid.

Materials and Experimental Methods

Materials

Amberlite 252 (Rohm & Haas Co.), the resin used in this study, is a macroreticular, sulfonated polystyrene-divinylbenzene resin. The physical properties of this material are summarized in Table 1. The total ion-exchange capacity was determined by letting a sample of hydrogen-form resin reach equilibrium with an excess volume of a 0.1 mol/L sodium hydroxide solution containing 50 g/L sodium chloride. After equilibrium was reached, the excess sodium hydroxide left in solution was titrated with a 0.1 mol/L hydrochloric acid solution and the capacity of the resin determined from a material balance. All chemicals used were analytical reagent grade (Fisher Scientific Co.). The water content of fully swollen resin particles was determined from the weight loss of weighed samples that occurred by drying in a vacuum oven at 110°C. The water content determined in this manner includes both hydration water and water that is trapped in the pores between microparticles (Patell and Turner, 1979). The arithmetic average particle diameter was determined by sorting a sample of wet resin with the aid of an optical microscope. The internal structure of Amberlite 252 was studied by means of scanning electron microscopy (SEM) (Patell and Turner, 1979; Campbell, 1987), which revealed that under a very thin layer of more uniform material on the outer surface, the resin consists of a macroporous conglomerate of microparticles that are held together to form a macrobead. As pointed out by Patell and Turner (1980), the effects of this surface layer on diffusion of ions into the resin particles are small, since the pores in this skin layer are still sufficiently wide to permit unhindered movement of small mole-

cules. The average size for the microparticles was estimated to be of the order of 0.05 μm. From the SEM studies, however, it is clear that the microparticles cannot be regarded as isolated entities; they are intimately interconnected to constitute a three-dimensional porous network. The resin macroporosity was estimated from the total water content of the resin by assuming that the microparticles contain an amount of water equal to that of a gel-type resin with the same degree of cross-linking and exchange capacity. The value of 0.75 g water/g dry resin obtained by Reichenberg and McCauley (1955) was used for this calculation.

The resin was pretreated by repeated washes with NaOH and HCl solutions, converted to the hydrogen form with 1 N HCl, and thoroughly rinsed with distilled deionized water. For experiments aimed at the determination of rates of mass transfer, small samples of pretreated wet resin were hand-picked with the aid of an optical microscope with particle diameters of 0.05 $\pm$ 0.002 and 0.1 $\pm$ 0.004 cm. Resin samples with mixed particle sizes were also used in some of the experiments; the average particle diameter in this case was approximately 0.08 cm, but a few particles as small as 0.005 cm and a few as large as 0.12 cm were present. In either case, the shape of the resin particles was very nearly spherical.

The amino acids studied in this work were L-phenylalanine (Phe) and L-tyrosine (Tyr). Both amino acids were obtained in crystalline form from Sigma and used without further purification. The concentrations of Phe and Tyr in aqueous solutions were determined colorimetrically with a spectrophotometer (Beckman, model DU-50). For solutions containing both species, the concentrations of Phe and Tyr were determined by HPLC. The concentrations of hydrogen and sodium ions in solution were obtained by means of pH and sodium-selective probes. Ion chromatography with electrical conductivity detection was also used to determine the sodium concentration in dilute samples. Distilled, deionized water was used to prepare all solutions.

Uptake equilibrium measurements

Equilibrium uptake isotherms were obtained for Phe and Tyr by means of batch equilibrium experiments carried out at constant ionic strength. For this purpose, varying amounts of dry resin (0.1 to 10 g) in the hydrogen form were allowed to reach equilibrium with known volumes of standard solutions (100–200 cm^3) containing an initial concentration of amino acid in sealed Erlenmeyer flasks. In addition to amino acid the solutions contained known amounts of chloride and sodium ions, which were added by dispensing volumes of standard HCl, NaCl, or NaOH. The flasks were placed in a constant-temperature shaker bath kept at 25 $\pm$ 1°C for 24 to 36 h. Liquid samples were withdrawn and analyzed either spectrophotometrically or by HPLC. The pH and sodium concentration of the solution after equilibrium was reached were also determined. The chloride concentration remained approximately constant during the process, since this species is nearly completely excluded from the resin microparticles by the Donnan potential effect at the low concentrations used in the experiments. The resin macropore volume accounted in all cases for less than 0.5% of the solution volume. Indirect proof that co-ion adsorption was negligible was given by the fact that calculated and predicted values of the solution pH before and after equilibration were in good agreement.

The equilibrium concentrations of amino acid and sodium in the resin phases were determined from material balances. Achievement of equilibrium was checked by taking repeated samples as well as by letting the system approach the same equilibrium state from the opposite direction, that is, by starting the experiments with resin loaded with amino acid. In all cases, the equilibrium uptake was expressed on a dry-resin basis.

Batch kinetics studies

Batch uptake experiments were carried out in the closed recirculated system sketched in Figure 2, which is similar to the apparatus described by Costa and Rodrigues (1985). A shallow layer of resin particles, approximately 0.5 cm thick and corresponding to about 0.35 g of resin (dry weight basis), was packed in a 1.5 cm dia. glass column with adjustable plungers (Spectrum Medical Products). The resin was packed between two 10 cm layers of glass beads with diameter matched to that of the resin sample being studied to insure an even distribution of the liquid flow. The shallow bed assembly was inserted in a liquid circulation loop comprising a positive displacement, constant-flow pump (FMI, model RHOCKC), a 200 cm^3 reservoir, a flow-through pH probe, and a flow-through UV cuvette. The reservoir was mixed with a magnetic stirrer. Signals from a spectrophotometer (Beckman, model DU-50) and a pH meter (Orion, model 701A) were recorded by a microcomputer (AT&T PC-6300) by means of a data acquisition board (Data Translation, DT-2805). The UV absorbance readings were converted to concentrations by means of calibration curves.

The circulation rate was varied between 10 and 120 cm^3/min. When the circulation rate is sufficiently high, the shallow bed provides differential contact and the system closely approximates a mixed batch system. To carry out a batch uptake run, the resin was converted to the hydrogen form and an HCl solution of the concentration desired for the experiment was pumped through the bed until steady conditions were reached. To start an adsorption experiment, the loop reservoir was charged with a solution containing a known amino acid concentration and the same HCl concentration as the solution being pumped through the bed. A rapid concentration step was then obtained by switching the valves and converting the system from an open one to a closed batch in which the reservoir solution is continuously circulated. Desorption experiments were carried out in a similar manner by initially loading the shallow bed with an amino acid

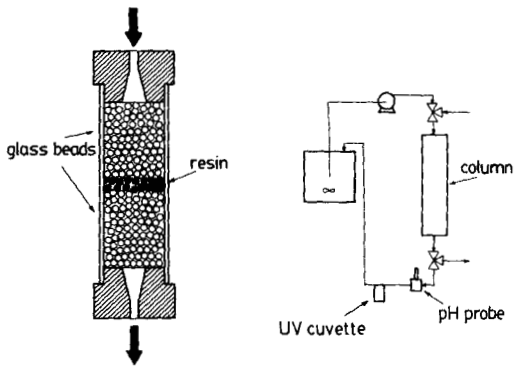

Figure 2. Shallow bed apparatus for transient uptake measurements.

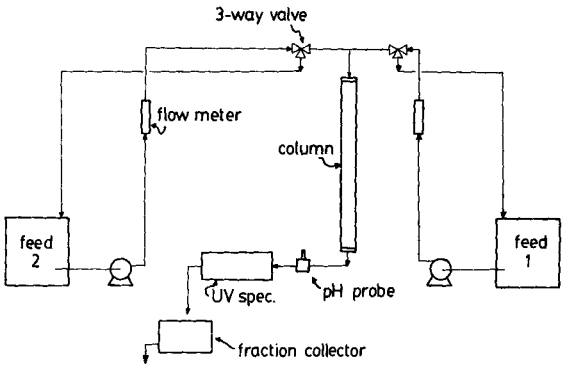

Figure 3. Apparatus for breakthrough and elution experiments.

solution of the desired concentration, and then replacing the circulating fluid with an HCl solution that initially contained no amino acid. Various particle sizes and solution concentrations were used in the experiments in order to fully characterize the mass transfer mechanism. All experiments were carried out at 25 ± 2°C.

The shallow-bed apparatus proved superior to a stirred vessel used in preliminary experiments. The shallow bed, in fact, provides good particle-fluid contact with a fairly well defined and reproducible fluid dynamics. Since conditions are similar to those of typical fixed-bed experiments, the external particle-fluid mass transfer coefficient may be accurately estimated using existing correlations for fixed beds. Furthermore, the arrangement eliminates solid-solid attrition problems that are encountered in stirred systems.

Fixed-bed breakthrough and elution studies

Breakthrough and elution experiments were carried out with the apparatus shown schematically in Figure 3. The resin particles, with an average diameter of 0.08 cm, were slurry-packed in a 1.5 cm dia., 40 cm long glass column (Spectrum Medical Products). Two layers of glass beads were used at the top and at the bottom of the bed to insure even flow of liquid. Two three-way valves were used to divert to the column the desired solutions, which were delivered by positive displacement pumps (FMI, model RHOCKC). The column effluent passed through a flow-through pH probe and a flow-through UV cuvette. Samples of the effluent were also collected at suitable time intervals with a fraction collector (Gilson, model 201). Operation of the apparatus was overseen by a microcomputer-based data acquisition and control system (AT&T PC-6300 microcomputer with a Data Translation model DT-2805 acquisition board). The experiments were run at 25 ± 2°C. The bed void fraction was estimated using a dilute solution of blue dextran with a molecular weight of 2,000,000 as a tracer, and was found to be 0.35 ± 0.02 for the hydrogen form of the resin. The resin density of the packed bed was obtained at the end of a series of experiments by emptying the column and determining the dry weight of the resin.

Results and Discussion

Na/H exchange equilibrium

Experimental data for the exchange of Na^+ and H^+ ions on Amberlite 252 are shown in Figure 4. The ionic fraction of sodium in solution was calculated from

$$X_{Na} = \frac{C_{Na^+}}{C_{Na^+} + C_{H^+}} \tag{11}$$

and the ionic fraction in the resin from

$$Y_{Na} = \frac{q_{Na}}{q_o} \tag{12}$$

where q_{Na} is the total amount of sodium taken up by the resin and q_o is the ion-exchange capacity of the resin. Since the amount of sodium taken up was determined from a material balance for the solution surrounding the resin, q_{Na} includes both the amount of sodium that is exchanged as well as that which is held within the resin pores. However, because the solutions used were rather dilute (less than 0.1 mol/L), q_{Na} should closely represent the amount of sodium ionically bound to the resin. Patell and Turner (1979) have investigated co-ion sorption (Cl^-) by Amberlite 252 from NaCl and HCl solutions. At concentrations less than 1 mol/L, co-ion uptake was found to be less than 0.02 mmol/g dry resin, which is less than 0.4% of the resin ion-exchange capacity.

A line representing the data of Patell and Turner (1979) is also shown in Figure 4. There is a slight discrepancy between the two sets of data, which may have resulted from slight differences occurring in the manufacture of the two lots of resin. The pretreatment procedures used may also have affected the exchange equilibrium measurements to some extent. Both sets of data, however, show that the apparent selectivity coefficient for the ion exchange of Na and H ions, defined by the following equation

$$S_{Na,H} = \frac{Y_{Na} X_H}{Y_H X_{Na}} \tag{13}$$

is greater than unity when the resin is almost entirely in the hydrogen form and reaches values slightly below unity when the resin is almost completely converted to the sodium form. Nonconstant selectivity coefficients are encountered in many resin systems, even at constant ionic strength (Helfferich, 1962; No-

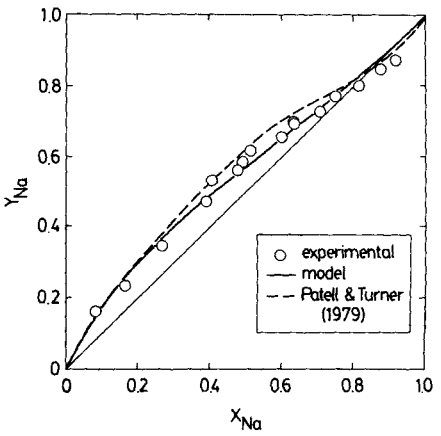

Figure 4. Ion-exchange equilibrium for Na^+/H^+ binary.
$C_{Cl^-} = 0.01$ mol/L.

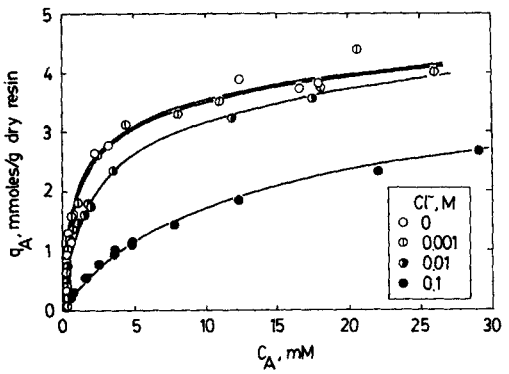

Figure 5. Uptake of Phe as a function of total concentration of amino acid in solution at various chloride ion concentrations.

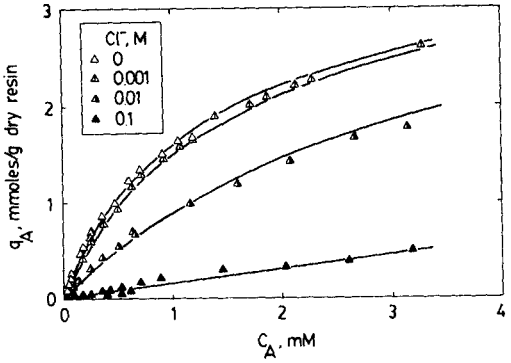

Figure 6. Uptake of Tyr as a function of total concentration of amino acid in solution at various chloride ion concentrations.

vosad and Myers, 1982; Soldatov and Bichkova, 1984; Myers and Byington, 1986). This effect may be attributed to inhomogeneities in the resin structure and functional groups, and is particularly significant for resins with a large degree of cross-linking.

Amino acid uptake equilibrium

The equilibrium uptake of Phe and Tyr by Amberlite 252 in the hydrogen form is shown in Figures 5 and 6. q_A represents the total amount of amino acid taken up by the resin, and C_A is the total concentration of amino acid in solution at equilibrium. The data were obtained for various concentrations of the co-ion Cl^-. Since in each experiment the co-ion concentration remained approximately constant, the pH varies from point to point on each curve, in the manner illustrated, for example, by Figure 1. If the total amino acid concentration is constant, as the chloride concentration is increased the pH decreases. As a result, the uptake of amino acid by the resin is reduced, because of the competition by hydrogen ions for the resin functional groups. If the chloride concentration is small or zero, the solution pH approaches the isoelectric pH of the amino acid. In this case, the dipolar form of the amino acid is predominant and hydroxyl ion may be present in significant concentration. Although only a very small fraction of the amino acid present in solution is protonated for these conditions, the uptake of amino acid by the resin is at a maximum because competition from hydrogen ions is minimized.

The behavior of Phe and Tyr is qualitatively quite similar since, at the acidic pH values of the data shown in Figures 5 and 6, the side chain of Tyr is not ionized and does not affect the ion-exchange process in a direct way. Data for Tyr, however, could only be obtained at low concentration because of its low solubility in aqueous solutions.

The uptake data for Phe and Tyr shown in Figures 5 and 6 are replotted in Figures 7 and 8 in the form normally used for ion-exchange equilibria. Equations 3–5 were used to compute the ionic fraction of amino acid cations in solution, X_A. The ionic fraction of amino acid cations in the resin, Y_A, was calculated from

$$Y_A = \frac{q_A}{q_o} \tag{14}$$

When the data are plotted in this form it is apparent that a single line correlates the uptake of amino acid at different co-ion concentrations and different pH values. Since the uptake of amino acid is dependent only upon the ionic fraction of amino acid cations in solution, it may be concluded that ion exchange is the predominant uptake mechanism. Nonionic adsorption does not appear to occur to a significant extent for the concentration

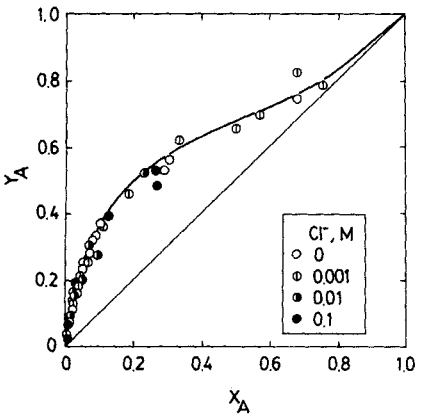

Figure 7. Ion-exchange equilibrium for Phe^+/H^+ binary.

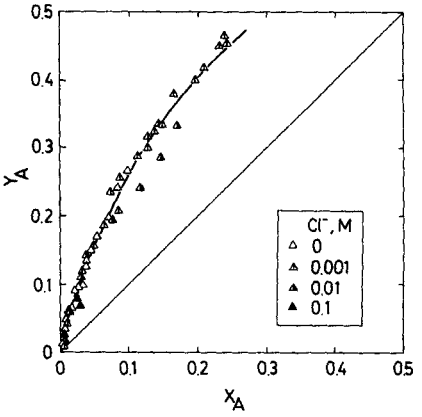

Figure 8. Ion-exchange equilibrium for Tyr^+/H^+ binary.

range investigated in this work. In a manner similar to the Na/H equilibrium, the selectivity coefficient for exchange of amino acid cations and hydrogen ions

$$S_{A,H} = \frac{Y_A X_H}{Y_H X_A} \tag{15}$$

decreases for Phe from values that are well above unity when X_A is small, to values approaching unity when X_A nears 1. The selectivity coefficient for Tyr also appears to decrease as X_A increases, although only the range of X_A from 0 to about 0.3 was investigated.

Ion-exchange equilibrium model

Variable selectivity coefficients for ion exchange found in this work can be attributed to inhomogeneities in the structure of the polymer and in the strength of the functional groups (Patell and Turner, 1979). The degree of cross-linking of the resin can be expected to be higher near the center of the microspheres than on their outer surface as a result of the polymerization conditions encountered during the manufacture of the resin. A variation in the acid strength of the functional groups within a resin may also result from the sulfonation process, which may cause oxidation of the polymer cross-linkages to form carboxylic acid groups. These groups contribute to the total ion-exchange capacity of the resin, but have an acid strength lower than the primary sulfonic acid groups.

As pointed out by Myers and Byington (1986), if the ion-exchange resin were homogeneous one would expect the selectivity coefficient to be approximately constant at constant ionic strength. Some deviation would of course be produced by non-idealities in the resin and bulk fluid phases, but these deviations would be expected to be only minor. If, on the contrary, the resin contains both high and low energy functional groups, a decrease in the selectivity for the ion preferred by the resin would be noted as the ionic fraction of that species is increased. This is observed for Na, Phe, and Tyr as shown in Figures 4, 7, and 8.

Barrer and Meier (1959) have proposed a two-site model to correlate variable selectivity ion-exchange data. More recently, Novosad and Myers (1982) and Myers and Byington (1986) have developed a general framework for ion-exchange isotherms based on an assumed continuous or discrete distribution of functional groups. In this approach, the ion-exchange process is regarded as the result of the competitive adsorption of ions onto the functional groups of the resin. The model assumes a binomial distribution of $n + 1$ site types having a characteristic energy level $E_{l,j}$, for the adsorption of an ion j on a site l. The probability of finding a site of type l is defined by

$$p_l = \binom{n}{l} p^l (1-p)^{n-l}, \quad 0 < p < 1 \tag{16}$$

$E_{l,j}$ is given by

$$E_{l,j} = \bar{E}_j + \frac{l - np}{\sqrt{np(1-p)}}\sigma_j \tag{17}$$

where $\bar{E}_j$ and σ_j are the average and the standard deviation of the distribution of adsorption energies, and p is the skewness of the site distribution function. When $p = 0.5$ the distribution of energies is symmetrical, while the distribution is skewed when p approaches 0 or 1. If the functional groups of the resin are completely dissociated, which is a reasonable assumption for a sulfonic acid resin, the following equation may be written to represent the adsorption of ion j onto site l

$$\frac{q_{l,j}}{q_{lo}} = \frac{C_{l,j}X_j}{\sum_{j=1}^{N} C_{l,j}X_j} \tag{18}$$

where q_{lo} is the number or concentration of sites l ($=q_o p_l$) and N is the number of exchangeable counterions. The $C_{l,j}$ values may be expressed in terms of the adsorption energy as

$$C_{l,j} = \bar{C}_j \exp\left(\frac{E_{l,j} - \bar{E}_j}{RT}\right) \tag{19}$$

Finally, the total uptake of ion j by the resin may be found by carrying out the summation over the $n + 1$ sites

$$\frac{q_j}{q_o} = \sum_{l=0}^{n}\left(\frac{C_{l,j}p_l X_j}{\sum_{j=1}^{N} C_{l,j}X_j}\right) \tag{20}$$

Myers and Byington have given a closed-form expression for the selectivity coefficient for a system containing two counterions, when $n = 1$. This expression may be easily extended to the case of N counterions. Choosing counterion j as the reference ion, the selectivity coefficient for ion i relative to ion j is given by

$$S_{i,j} = \frac{Y_i X_j}{Y_j X_i} = \bar{S}_{i,j}\frac{\sum_{k=1}^{N}\{\bar{S}_{k,j}X_k W_{k,j}^{U+V}[(1-p)W_{i,k}^{U} + pW_{i,k}^{V}]\}}{\sum_{k=1}^{N}\{\bar{S}_{k,j}X_k W_{k,j}^{U+V}[(1-p)W_{j,k}^{U} + pW_{j,k}^{V}]\}} \tag{21}$$

where

$$\bar{S}_{i,j} = \exp\left(\frac{\bar{E}_i - \bar{E}_j}{RT}\right) \tag{22}$$

$$W_{i,j} = \exp\left(\frac{\sigma_i - \sigma_j}{RT}\right) \tag{23}$$

$$U = \frac{-p}{\sqrt{p(1-p)}} \tag{24}$$

$$V = \frac{1-p}{\sqrt{p(1-p)}} \tag{25}$$

Once all the $S_{i,j}$ are determined the uptake of ion i may be computed from

$$Y_i = \frac{q_i}{q_o} = \frac{X_i S_{i,j}}{\sum_{k=1}^{N} X_k S_{k,j}} \tag{26}$$

As shown by Myers and Byington, Eqs. 21–26 constitute an ion-exchange isotherm that is thermodynamically consistent and

Table 2. Equilibrium Parameters for Amberlite 252*

	pK_1	pK_2	pK_3	$\bar{S}$	W	p
L-Phe	2.11	9.13	—	3.2	4.9	0.61
L-Tyr	2.20	9.11	10.1	2.1	3.7	0.61
Na	—	—	—	1.5	0.39	0.61

*Reference counterion: H^+; co-ion: Cl^-

which may be applied to the prediction of multicomponent ion-exchange equilibria, provided that resin and solution phase non-ideality effects are small. If a value of the skewness parameter p is selected for the resin, then for each binary system the model contains the two parameters $\bar{S}$ and W. Thus, data on $N-1$ binary systems are required to make predictions of equilibrium in a system consisting of N counterions.

In applying Eqs. 21–26 to our system, we determined the best fit values of p, $\bar{S}$, and W for each binary Na/H, Phe/H, and Tyr/H. In each case H^+, which is the least preferred species, was used as the reference ion. This procedure provided values of p that were different for each binary. Since a single value of p is desired in order to make multicomponent predictions, the values of p, $\bar{S}$, and W determined for the binaries were used as initial guesses in a nonlinear least-squares fitting routine, which determined the best values of the parameters for all three binaries using a single value of p. This procedure yielded the parameter values given in Table 2. Figures 4–8 show lines calculated from Eqs. 21–26 with these parameters. The correlation appears to be well within experimental error in all cases studied.

Multicomponent ion-exchange equilibrium

Multicomponent equilibrium measurements were carried out for the systems Phe/Na/H, Tyr/Na/H, and Phe/Tyr/H using the static shaker-flask method, and are shown in Tables 3, 4, and 5.

The agreement between experimental results and model calculations is generally quite good. Theoretical predictions are in all cases within ±20% of the experimental observations, which is approximately the experimental accuracy of the determination

Table 3. Phe/Na/H Equilibrium

C_{Cl^-} mmol/L	C_{Phe} mmol/L	C_{Na^+} mmol/L	pH^{exp}	pH^{calc}	X_{Phe}	X_{Na}	Y^{exp}_{Phe}	Y^{calc}_{Phe}	Y^{exp}_{Na}	Y^{calc}_{Na}
4	0.540	0.156	2.45	2.44	0.043	0.039	0.228	0.216	0.068	0.067
	1.08	0.134	2.46	2.45	0.084	0.034	0.332	0.328	0.068	0.067
	1.88	0.191	2.50	2.49	0.139	0.048	0.434	0.419	0.067	0.080
	7.56	0.161	2.70	2.66	0.414	0.040	0.658	0.621	0.068	0.080
	18.3	0.150	2.94	2.90	0.644	0.038	0.760	0.723	0.068	0.090
11	0.850	1.17	2.05	2.03	0.042	0.106	0.218	0.214	0.210	0.185
	1.67	1.25	2.07	2.05	0.081	0.114	0.316	0.321	0.206	0.182
	2.88	1.32	2.12	2.09	0.135	0.120	0.406	0.412	0.206	0.186
	9.91	1.59	2.34	2.27	0.368	0.145	0.596	0.581	0.200	0.216
	33.8	1.56	2.76	2.67	0.664	0.142	0.756	0.684	0.200	0.235
26	2.98	7.66	1.81	1.79	0.077	0.299	0.284	0.320	0.406	0.341
	14.4	9.16	2.11	2.04	0.300	0.352	0.492	0.540	0.372	0.343
	37.4	9.02	2.52	2.40	0.496	0.347	0.670	0.611	0.368	0.344
51	2.53	24.5	1.61	1.61	0.038	0.480	0.178	0.212	0.592	0.487
	17.7	27.6	1.98	1.90	0.214	0.541	0.416	0.498	0.518	0.422
	43.5	27.1	2.39	2.25	0.358	0.531	0.534	0.560	0.520	0.404
101	6.43	68.1	1.60	1.56	0.050	0.674	0.206	0.265	0.732	0.678
	21.4	71.0	1.91	1.81	0.142	0.703	0.330	0.441	0.662	0.500
	47.0	70.1	2.30	2.12	0.231	0.694	0.454	0.513	0.668	0.464

Table 4. Tyr/Na/H Equilibrium

C_{Cl^-} mmol/L	C_{Tyr} mmol/L	C_{Na^+} mmol/L	pH^{exp}	pH^{calc}	X_{Tyr}	X_{Na}	Y^{exp}_{Tyr}	Y^{calc}_{Tyr}	Y^{exp}_{Na}	Y^{calc}_{Na}
1	0.437	0.276	3.07	3.17	0.043	0.276	0.142	0.141	0.284	0.362
	0.850	0.110	3.10	3.10	0.095	0.110	0.268	0.252	0.182	0.185
	1.69	0.077	3.10	3.13	0.178	0.077	0.392	0.373	0.147	0.140
	3.16	0.064	3.15	3.19	0.292	0.064	0.546	0.481	0.137	0.124
	2.06	0.177	3.17	3.20	0.188	0.177	0.430	0.383	0.290	0.254
10	19.4	2.01	2.18	2.16	0.102	0.201	0.265	0.266	0.326	0.282
	2.18	2.83	2.24	2.21	0.107	0.283	0.273	0.278	0.349	0.349
	2.41	3.71	2.30	2.28	0.109	0.371	0.271	0.284	0.470	0.409
	2.62	4.98	2.43	2.40	0.102	0.498	0.263	0.278	0.551	0.488
	1.82	0.901	2.11	2.09	0.102	0.090	0.269	0.266	0.326	0.282
11	0.272	8.83	2.70	2.68	0.006	0.803	0.033	0.029	0.753	0.807
	0.624	9.07	2.77	2.75	0.013	0.825	0.069	0.056	0.755	0.807
	0.969	8.95	2.78	2.74	0.020	0.814	0.087	0.085	0.773	0.781
	1.30	8.99	2.80	2.76	0.025	0.817	0.112	0.106	0.749	0.771
	1.69	9.11	2.85	2.81	0.030	0.828	0.111	0.123	0.723	0.769

Table 5. Phe/Tyr/H Equilibrium

C_{Cl^-} mmol/L	C_{Phe} mmol/L	C_{Tyr} mmol/L	pH^{exp}	pH^{calc}	X_{Phe}	X_{Tyr}	Y^{exp}_{Phe}	Y^{calc}_{Phe}	Y^{exp}_{Tyr}	Y^{calc}_{Tyr}
1	0.390	0.432	*	3.04	0.041	0.055	0.176	0.184	0.131	0.123
	0.940	0.461	*	3.07	0.094	0.055	0.330	0.309	0.101	0.097
	1.15	1.10	*	3.11	0.106	0.121	0.306	0.295	0.191	0.182
	1.40	1.05	*	3.12	0.126	0.113	0.342	0.332	0.167	0.162
	1.77	1.60	*	3.16	0.147	0.159	0.342	0.340	0.212	0.202
	1.63	0.887	3.10	3.12	0.097	0.100	0.296	0.250	0.180	0.160
	2.24	0.992	3.16	3.15	0.190	0.101	0.448	0.421	0.130	0.120
	4.20	1.19	3.25	3.31	0.302	0.103	0.514	0.520	0.120	0.100
	6.38	1.50	3.31	3.30	0.390	0.110	0.540	0.570	0.100	0.094
	1.08	0.638	3.09	3.09	0.104	0.074	0.339	0.316	0.083	0.120
	1.02	1.08	3.15	3.10	0.094	0.120	0.302	0.379	0.156	0.189
	1.16	1.60	3.16	3.14	0.101	0.101	0.293	0.266	0.236	0.239
	1.17	2.21	3.19	3.16	0.096	0.217	0.275	0.239	0.292	0.295

*Not determined

of the concentration of sodium in our amino acid mixtures. For the Phe/Na/H system, however, while the agreement is good at low values of Y_{Phe} and Y_{Na}, significant deviations are found at higher values of Y_{Na}. This may result from resin and solution phase nonidealities and, especially, from inaccuracies in the determination of the fitting parameters, which were based on data obtained predominantly for low values of Y_{Na} and Y_{Phe}.

The uptake of Phe and Tyr by Amberlite 252 was also studied at alkaline pH values in the presence of Na, and Figure 9 shows the full effect of the equilibrium pH value on the uptake of Phe. This figure refers to batch experiments carried out with a constant total amount of Phe in a closed, agitated vessel. The experiments were started at a solution pH value of about 4.6. In one set of experiments, shown to the left of the initial conditions in Figure 9, the solution pH was gradually reduced by small additions of concentrated HCl. In this case, the amount of Phe taken up by the resin decreases as the pH is reduced, due to the increased competition by hydrogen ions. In the other set of experiments, which are shown to the right of the initial condition, the solution pH was gradually increased by adding small amounts of concentrated NaOH. Here the uptake of Phe by the resin drops very quickly as a result of the competition by Na ions, and especially as a result of the conversion of Phe to the negatively charged form. The latter form appears to be completely excluded from the resin and at pH values significantly higher than the isoelectric pH of Phe the uptake is essentially zero. As is apparent from this figure, when more than one counterion is present the amount of amino acid taken up by the resin has a maximum value at some solution pH value. The latter can be determined easily by means of Eqs. 3–5 and 21–26 if the solution composition is known.

External mass transfer: Na/H exchange

The external mass transfer resistance in the shallow bed was determined by measuring the rate of uptake of NaOH from dilute solutions by the hydrogen form of the resin. Figure 10 shows the experimental concentration history for batch uptake from a 0.01 mol/L NaOH solution. As shown by Helfferich (1965), when external film diffusion controls, as long as the bulk solution concentration of NaOH is well above 10^{-7} mol/L, H^+ released from the resin does not make headway into the film but is consumed right at the particle surface by reaction with OH^- to form water. The hydrogen ion concentration at the particle surface thus remains very small and diffusion of NaOH through the external film occurs with a constant diffusion coefficient. For these conditions, which hold until conversion of the resin to the Na form is almost complete, the Na solution concentration

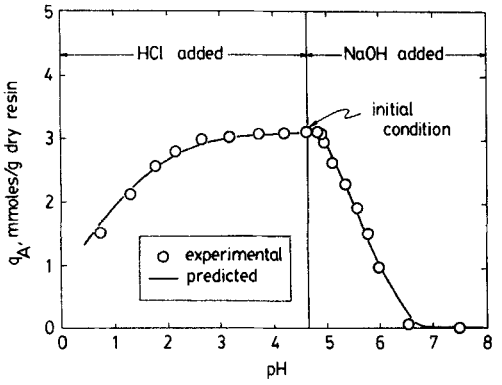

Figure 9. Effect of pH on uptake of Phe in a closed system.
Solution volume = 100 cm³; resin mass = 1.96 g dry resin, total amount Phe = 6.07 mmol.

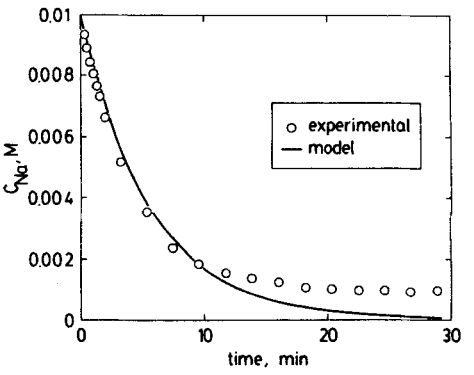

Figure 10. Concentration history for transient uptake of Na from 0.01 mol/L NaOH.
Solution volume = 200 cm³; resin mass = 0.382 g dry resin; circulation rate = 115 cm³/min

in the batch system may be approximately expressed as

$$C_{Na^+} = C^o_{Na^+} \exp\left(-\frac{k_f a V_b}{V_s} t\right) \tag{27}$$

where $C^o_{Na^+}$ is the initial Na concentration, k_f is the external film mass transfer coefficient, a is the interfacial area, and V_b and V_s are the volumes of the resin bed and of the solution, respectively. The external mass transfer coefficient may be estimated from empirical expressions for mass transfer to spheres in fixed beds. We used the following equation for mass transfer to ion-exchange resins (Kataoka et al., 1973) to estimate k_f

$$\frac{\epsilon k_f}{u} = 1.85\left(\frac{\epsilon}{1-\epsilon}\right)^{1/3}(Re)^{-2/3}(Sc)^{-2/3} \tag{28}$$

where Re and Sc are the Reynolds and Schmidt numbers, u is the fluid superficial velocity, and ϵ is the void fraction of the resin bed. The interfacial area of the resin was estimated according to

$$a = \frac{3(1-\epsilon)}{R} \tag{29}$$

Calculations based on Eqs. 27–29 were found to be in good agreement with experimental measurements, as shown in Figure 10. The agreement is of course not good when conversion of the resin to the sodium form is almost complete, since for these conditions the model assumptions are infringed.

Internal mass transfer: kinetic models for exchange of amino acids

Intraparticle mass transfer occurs by parallel diffusion through the liquid-filled macropores of the resin and through the microparticles. A simplified kinetic model for the uptake of amino acids by the hydrogen form of the resin, was developed based on the following assumptions:

1. Amino acid cations can freely diffuse through the microparticles, while diffusion of both amino acid cations and zwitterions takes place in the macropores. Diffusion of the zwitterions through the microparticle is neglected since these molecules do not appear to be significantly adsorbed by the resin and the solid diffusivities are expected to be much smaller than the corresponding macropore values.
2. Co-ions (in our experimental investigation we used Cl^-) are also free to penetrate the resin macropores, but are excluded from the microparticles by the Donnan potential effects.
3. The solution pH remains below the isoelectric pH, so the presence of negatively charged amino acid molecules may be neglected.
4. The resin particles are spherical, with a uniform porous structure composed of a rigid lattice of macropores and microparticles.
5. Local equilibrium exists between the fluid contained in the macropores and the microparticles.

The following conservation equations may be written for the diffusion of amino acid, A, and the co-ion Cl^-

$$\epsilon_p \frac{\partial c_A}{\partial t} + (1-\epsilon_p)\frac{\partial q'_A}{\partial t} = -\frac{1}{r^2}\frac{\partial}{\partial r}\left[r^2(J_{A^+} + J_{A^\pm} + \bar{J}_{A^+})\right] \tag{30}$$

$$\epsilon_p \frac{\partial c_{Cl^-}}{\partial t} = -\frac{1}{r^2}\frac{\partial}{\partial r}(r^2 J_{Cl^-}) \tag{31}$$

where c_A and q'_A are the concentrations of total amino acid in the macropore and in the microparticles, respectively, J_{A^+} and $\bar{J}_{A^+}$ are the fluxes of amino acid cation in the macropore and microparticles, and $J_{A^\pm}$ and J_{Cl^-} are the fluxes of dipolar amino acid and chloride ions in the macropore. q' is defined per unit volume of microparticles. The fluxes may be represented by the Nernst-Planck equations given by

$$J_{i^+} = -D_{i^+}\left(\frac{\partial c_{i^+}}{\partial r} + \frac{c_{i^+}F}{RT}\frac{\partial \phi}{\partial r}\right) \quad \text{for } i = A, H \tag{32}$$

$$J_{A^\pm} = -D_{A^\pm}\left(\frac{\partial c_{A^\pm}}{\partial r}\right) \tag{33}$$

$$J_{Cl^-} = -D_{Cl^-}\left(\frac{\partial c_{Cl^-}}{\partial r} - \frac{c_{Cl^-}F}{RT}\frac{\partial \phi}{\partial r}\right) \tag{34}$$

$$\bar{J}_{i^+} = -\bar{D}_{i^+}\left(\frac{\partial q'_i}{\partial r} + \frac{q'_{i^+}F}{RT}\frac{\partial \phi}{\partial r}\right) \quad \text{for } i = A, H \tag{35}$$

where ϕ is the electrical potential and the D_i's are effective diffusivities of the various ionic species. The following conditions of electroneutrality and no net electric current apply

$$c_{A^+} + c_{H^+} = c_{Cl^-} \tag{36}$$

$$q'_A + q'_H = q'_o \tag{37}$$

$$J_{A^+} + J_{H^+} = J_{Cl^-} \tag{38}$$

$$\bar{J}_{A^+} + \bar{J}_{H^+} = 0 \tag{39}$$

Equations 32–35 can be combined with Eqs. 36–39 to eliminate the electrical potential and obtain closed-form expressions for the fluxes as functions of the concentration gradients. However, in the uptake of amino acids the solutions typically encountered are dilute and the effects of the electrical potential on macropore diffusion of amino acid may be neglected. In this case, in fact, where the co-ion concentration is very small, the pH approaches the isoelectric pH of the amino acid and the zwitterion form is largely dominant. Thus, Eq. 33 accounts almost entirely for the total flux of amino acid through the macropore. At higher co-ion concentrations diffusion of amino acid cations and zwitterions occur in parallel through the macropore. However, for these conditions the concentration of hydrogen ion is ordinarily much larger than the concentration of amino acid cation, and the latter almost completely controls the coupled diffusion process. Similar considerations apply to diffusion of amino acid through the external film, but not to diffusion through the microparticles where concentrations of A^+ and H^+ of comparable magnitude are found.

With the above assumptions, and taking $D_{A^+} = D_{A^\pm} = D_A$, Eq. 30 becomes

$$\epsilon_p \frac{\partial c_A}{\partial t} + (1-\epsilon_p)\frac{\partial q'_A}{\partial t} = \frac{1}{r^2}\frac{\partial}{\partial r}\left[r^2\left(D_A\frac{\partial c_A}{\partial r} + \bar{D}_A\frac{\partial q'_A}{\partial r}\right)\right] \tag{40}$$

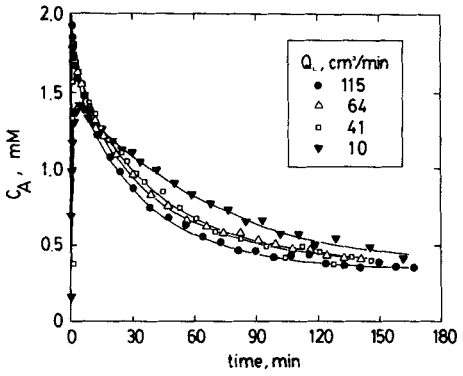

Figure 11. Effect of circulation rate on transient uptake of Phe.
Run nos. 10, 11, 12, 13

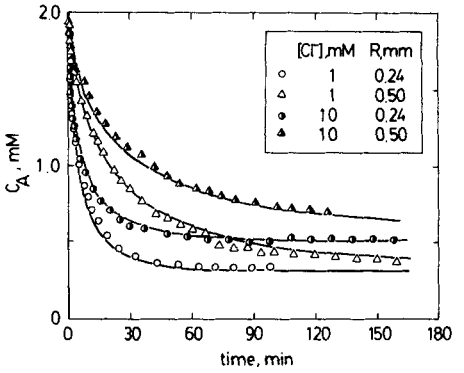

Figure 12. Experimental results and model calculations for transient uptake of Phe.
Run nos. 2, 4, 6, 8

where

$$\bar{D}_A = \frac{\bar{D}_{A^+} \cdot \bar{D}_{H^+} \cdot q'_o}{\bar{D}_{A^+} \cdot q'_A + \bar{D}_{H^+} \cdot (q'_o - q'_A)} \tag{41}$$

q'_A is locally related to c_A by the equilibrium isotherm and is given by

$$q'_A = \frac{\rho_p}{1 - \epsilon_p} q_A(c_A, c_{Cl^-}) - \frac{\epsilon_p}{1 - \epsilon_p} c_A \tag{42}$$

Initial and boundary conditions are given by

$$c_A(r, 0) = c^o_A(r, 0) \tag{43}$$

$$\frac{\partial c_A}{\partial r}(0, t) = 0 \tag{44}$$

$$c_A(R, t) = C^i_A(t) \tag{45}$$

$$\left(D_A \frac{\partial c_A}{\partial r} + \bar{D}_A \frac{\partial q'_A}{\partial r}\right)_{r=R} = k_f[C_A(t) - C^i_A(t)] \tag{46}$$

where C^i_A is the sorbate concentration at the particle surface. In a finite-volume bath, the sorbate concentration in the fluid phase external to the particles, C_A, changes with time and is related to the flux by a material balance

$$\frac{dC_A}{dt} = -k_f a[C_A(t) - C^i_A(t)] \tag{47}$$

$$C_A(0) = C^o_A \tag{48}$$

The chloride concentration is assumed to be constant. Equations 40–48, coupled with the equilibrium uptake isotherm were solved numerically by orthogonal collocation on finite elements as illustrated in appendix A.

Analysis of batch uptake experimental results

Transient uptake experiments were carried out with various co-ion concentrations, particle sizes, and circulation rates. The experimental results were then compared with the numerical solution of the intraparticle diffusion model to determine the best fit values of the effective diffusivities D_A and $\bar{D}_{A^+}$. The value of the effective diffusivity of H^+ through the microparticles of 2.3×10^{-6} cm²/s, obtained by Patell and Turner (1980) for Amberlite 252 was used in the calculations. It is possible to differentiate between macropore and microparticle diffusion by carrying out experiments at different co-ion concentrations. As the co-ion concentration is increased, in fact, the equilibrium uptake of amino acid is decreased and macropore transport acquires greater importance.

Figure 11 shows the effect of circulation rate in the shallow-bed appartus on the transient uptake of Phe. The fluid phase concentration is plotted as a function of time for the different experiments. At the lowest circulation rate, the system deviates significantly from the behavior of a differential contactor, and a large concentration drop occurs across the bed during the initial stages of the uptake process. At the higher circulation rates, the apparatus effectively approximates a stirred-batch system. Furthermore, at these flow rates the uptake curves are essentially coincident, showing that external mass transfer must be important only during the early stages of the adsorption process. A circulation rate of 115 cm³/min was used for the bulk of the experiments.

Representative adsorption and desorption curves for Phe are shown in Figures 12, 13, and 14 for varying co-ion concentrations and particle sizes. The experimental conditions are given in

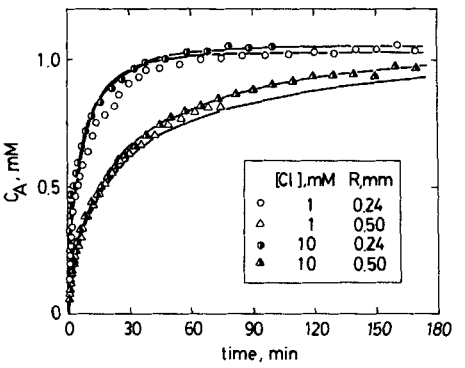

Figure 13. Experimental results and model calculations for transient desorption of Phe.
Run nos. 3, 5, 7, 9

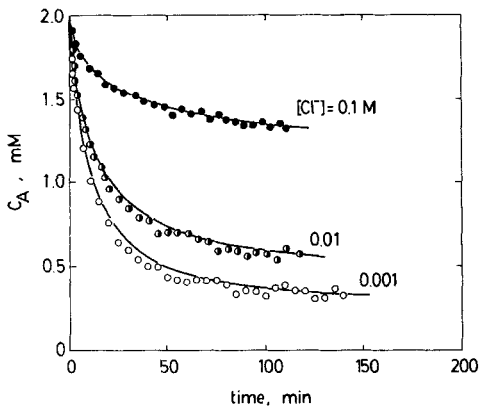

Figure 14. Experimental results and model calculations for transient uptake of Phe.
Mixed resin particles, 0.04 cm average radius.
Run nos. 14, 15, 16

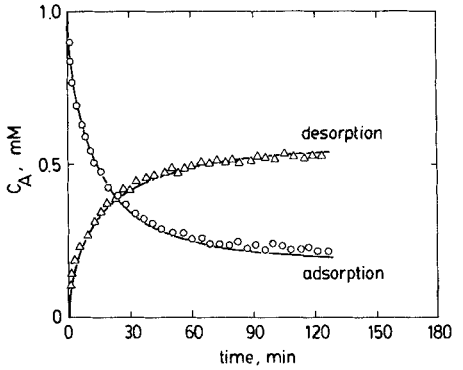

Figure 15. Experimental results and model calculations for transient uptake of Tyr.
Mixed resin particles, 0.04 cm average radius.
Run nos. 19, 20

Table 6. Lines calculated from the intraparticle diffusion model are also given in these figures. The values $D_A = 2.5 \times 10^{-6}$ cm^2/s and $\bar{D}_{A^+} = 1.4 \times 10^{-8}$ cm^2/s, which were determined from a fit of the experimental data, were used for these calculations. A more limited set of runs was also carried out for Tyr, and representative adsorption and desorption curves are given in Figure 15. The values of $D_A = 2.3 \times 10^{-6}$ cm^2/s and $\bar{D}_{A^+} = 1.8 \times 10^{-8}$ cm^2/s were obtained for Tyr. If the free diffusivities of Phe and Tyr calculated from the Wilke-Chang equation are assumed to be representative of macropore diffusion, using a particle porosity of 0.24, the values of D_A yield a tortuosity factor between 1.2 and 1.4. The effective diffusivity values for amino acid transport through the microparticles are however much smaller than the diffusivity of hydrogen ions. Thus, the overall diffusion coefficient $\bar{D}_A$ observed in our experiments is very close to the self-diffusivity of amino acid cations, except when hydrogen ions are nearly completely absent from the resin. While it is difficult to make exact comparisons with diffusivity values obtained for other resin types, these microparticle diffusivity values are found to be about an order of magnitude smaller than the diffusivity of monovalent cations, such as Na^+, for gel-type resins with a similar degree of cross-linking. The values found are instead close in magnitude to the diffusivities of divalent cations such as Zn^{++}, as obtained, for example, by Kataoka et al. (1974).

Table 6. Experimental Conditions for Batch Uptake Studies†

Run No.	Species	Resin Mass g dry	R cm	Flow Rate cm^3/min	C_A^o mmol/L	c_A^o mmol/L	$\bar{q}_A^\infty$ mmol/g	k_f cm/s $\times 10^{-2}$	C_{Cl^-} mmol/L
1	Phe	0.378	0.024	115	1.88	0	0.906	1.18	1
2	Phe	0.378	0.024	115	2.0	0	0.913	1.18	1
3	Phe	0.378	0.024	115	0	2.0	1.79	1.18	1
4	Phe	0.378	0.024	115	2.0	0	0.826	1.18	10
5	Phe	0.378	0.024	115	0	2.0	1.32	1.18	10
6	Phe	0.357	0.050	115	2.0	0	0.957	0.73	1
7	Phe	0.357	0.050	115	0	2.0	1.77	0.73	1
8	Phe	0.357	0.050	115	2.0	0	0.860	0.73	10
9	Phe	0.357	0.050	115	0	2.0	1.30	0.73	10
10	Phe	0.325	0.050	115	2.0	0	1.03	0.73	1
11	Phe	0.325	0.050	64	2.0	0	1.03	0.61	1
12	Phe	0.325	0.050	41	2.0	0	1.03	0.52	1
13	Phe	0.325	0.050	10	2.0	0	1.03	0.33	1
14	Phe	0.381	0.04*	115	2.0	0	0.897	0.86	1
15	Phe	0.381	0.04*	115	2.0	0	0.788	0.86	10
16	Phe	0.381	0.04*	115	2.0	0	0.381	0.86	100
17	Phe	0.357	0.04*	55	0	2.0	1.86	0.66	1
18	Phe	0.357	0.04*	115	0	2.0	1.86	0.96	1
19	Tyr	0.376	0.04*	115	1.0	0	0.430	0.82	1
20	Tyr	0.376	0.04*	115	0	1.0	1.14	0.82	1
21	Tyr	0.376	0.04*	115	1.0	0	0.361	0.82	10
22	Tyr	0.376	0.04*	115	0	1.0	0.581	0.82	10
23	Tyr	0.562	0.050	115	1.0	0	0.291	0.69	1

†Bed properties; $\epsilon = 0.35$, $\rho_b = 0.38$ g dry resin/cm^3, $V_s = 200$ cm^3
*Mixed particles, average radius.

The experimental data in Figures 12 and 13 were obtained for samples of resin with a nearly uniform particle size while Figures 14 and 15 correspond to samples of resin with the broader distribution of particle sizes that is typical of commercial resins. In this case, the arithmetic average particle diameter of wet resin was used. Experimental results and calculated curves are in all cases in excellent agreement, both for positive and negative concentration steps. In the adsorption experiments, as the co-ion concentration is reduced the ultimate solution concentration of amino acid, which is obtained for $t \rightarrow \infty$, decreases, because of the increased equilibrium uptake by the resin. The opposite occurs for the desorption experiments, although it is less noticeable since these experiments were conducted at a lower concentration level. The solution pH changes during the course of each run as the concentration of amino acid in solution changes and may be calculated from Eqs. 6 and 7.

The relative importance of external, macropore, and microparticle transport of amino acid is illustrated by the calculated uptake curves for Phe shown in Figure 16. The full model, including all three transport mechanisms, is compared here with calculations that assume no external mass transfer resistance ($k_f \rightarrow \infty$), or no macropore transport ($D_A = 0$). It is apparent that at the lower chloride concentration, when the equilibrium uptake of amino acid is high, transport of amino acid cations through the microparticles is the dominant mechanism. External film resistance is important only during the initial stages of the uptake process. At higher chloride concentrations, the equilibrium uptake of amino acid by the resin is reduced because of the increased competition of hydrogen ions with amino acid cations for the functional groups. For these conditions, macropore transport becomes a more significant contribution to the overall intraparticle transport process.

Fixed-bed behavior: dynamic model

Considering a uniformly packed bed of resin, with void fraction ϵ and resin density ρ_b, a differential balance for the amino acid solute A yields the following continuity equation

$$\epsilon \frac{\partial C_A}{\partial t} + \rho_b \frac{\partial \bar{q}_A}{\partial t} + u \frac{\partial C_A}{\partial z} = 0 \tag{49}$$

$\bar{q}_A$ is defined here as the adsorbed amino acid concentration averaged over the mass of the particle. Axial dispersion is neglected in this equation since its effects on the spreading of breakthrough and elution curves are small for our system in comparison with the effects of intraparticle and external film mass transfer resistances. Accumulation of amino acid in the resin at each point in the bed is given by

$$\rho_b \frac{\partial \bar{q}_A}{\partial t} = k_f a [C_A(z, t) - C_A^i(z, t)] \tag{50}$$

The interfacial concentration, C_A^i, is related to the intraparticle concentration gradients by Eq. 46. An additional continuity equation is in general needed to describe the motion of the co-ion through the fixed bed. In practice, however, since only the macropore is accessible to the co-ion, this species moves very rapidly through the bed. In this work, therefore, the co-ion concentration was assumed to be constant. The boundary condition for Eq. 49 is given by

$$C_A(0, t) = C_A^F(0, t) \tag{51}$$

where C_A^F is the concentration of amino acid in the feed. The intraparticle concentration, c_A, is now a function of z, r, and t.

Simultaneous solution of the intraparticle diffusion model, Eqs. 40–46, with Eqs. 49–51 was obtained by orthogonal collocation as illustrated in appendix B. While a constant-pattern solution can be more simply obtained to model breakthrough behavior, a general numerical solution provides the additional flexibility of allowing the prediction of pulse and elution response curves, and can readily be extended to multicomponent systems.

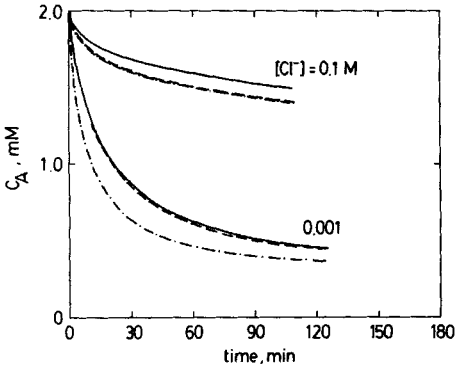

Figure 16. Calculated concentration histories for Phe using different transport mechanisms.
Calculations based on parameters for run no. 6.
— full model; --- $D_A = 0$; ···· $k_f \rightarrow \infty$

Analysis of breakthrough and elution curves

Breakthrough and elution curves were obtained, as described earlier, for various feed concentrations, flow rates, and for two bed heights. The experimental conditions for these runs are summarized in Table 7, and the experimental results are shown in Figures 17, 18, and 19, together with the calculated curves based on the intraparticle diffusion model. The parameters determined from the batch rate measurements were used in these calculations without further adjustment. The external mass transfer coefficient was calculated from Eq. 28. It is evident that the theoretical curves are in excellent agreement with the experimental results and that accurate predictions of the response of fixed beds to positive and negative feed concentration steps can be made. As in the batch experiments, while the Cl^- concentration remains approximately constant, the effluent

Table 7. Experimental Conditions for Fixed-bed Studies

	Run No.					
	1	2	3	4	5	6
Species	Phe	Phe	Phe	Phe	Tyr	Tyr
Bed length,* cm	37.0	37.0	24.4	24.4	24.4	24.4
u, cm/s	0.70	0.70	0.82	1.27	0.36	0.89
C_A^F, mmol/L	4.7	0	5.0	5.0	2.5	2.5
C_A^0, mmol/L	0	4.7	0	0	0	0
C_{Cl^-}, mmol/L	1.0	1.0	1.0	1.0	10	10
k_f, cm/s $\times 10^{-2}$	0.72	0.72	0.77	0.88	0.53	0.78

*Bed properties: $\epsilon = 0.35$, $\rho_b = 0.38$ g dry resin/cm^3; $R = 0.04$ cm

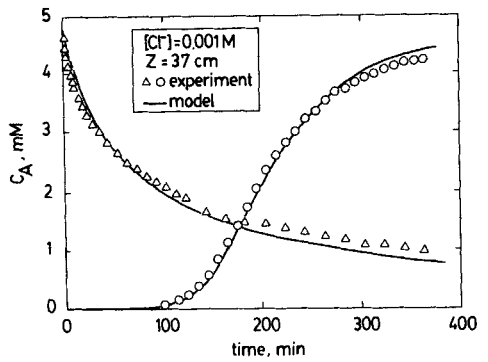

Figure 17. Experimental results and model predictions of breakthrough and elution curves for Phe.
Run nos. 1, 2

pH varies as the concentration of amino acid changes and can be calculated from Eqs. 6 and 7.

Conclusions

We have demonstrated that the uptake of amino acids by a cation-exchange resin may be accurately predicted by taking into account solution and ion-exchange equilibria. The amount of amino acid taken up by the resin appears to depend only upon the ionic fraction of amino acid cations in solution. Nonionic adsorption seems to be insignificant in the range of concentrations investigated. However, it is possible that hydrophobic interactions may be more significant, in a relative sense, at low amino acid concentrations, when the ion-exchange contribution is small.

A model for ion exchange involving N counterions has been developed. While this model does not take into account solution and resin phase nonidealities, it strikes a reasonable compromise between a rigorous thermodynamic treatment and the necessity of limiting the number of experimental measurements that are required to determine the appropriate parameters. The model allows the optimization of operating conditions for ion exchange of amino acids and can be used in the development of models for the design of separation processes. It should be noted, however, that in our treatment we have neglected the effects of solution nonidealities, since the solutions were rather dilute. For more concentrated solutions these effects may be taken into account by using appropriate activity coefficient models for the species present in the aqueous phase.

The results of our experimental rate measurements show that the intraparticle diffusion process is governed by diffusion of amino acid cations through the solid phase of the macroreticular resin. Macropore transport becomes more important at high co-ion concentrations, when the equilibrium uptake of amino acid is reduced. We have shown that equilibrium uptake, transport, and fixed-bed dynamics for the amino acid-resin system can be described by rational models that take into account the ionic properties of amino acid molecules. The feasibility of making accurate predictions of fixed-bed behavior on the basis of these models without using any additional fitting parameters has been demonstrated. This approach to modeling is very fundamental and requires a considerable amount of experimental information. The approach is very powerful, however, and superior to other techniques that require the fitting of lumped parameters.

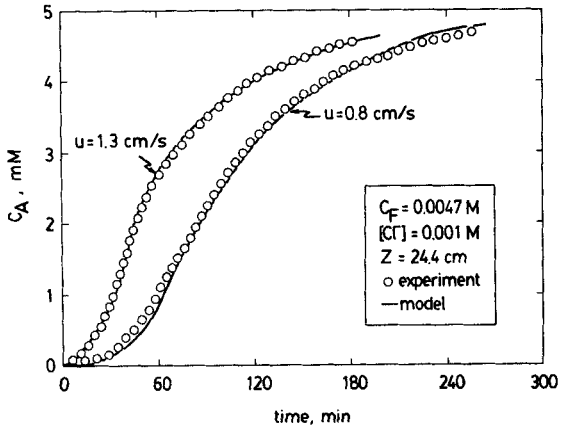

Figure 18. Experimental results and model predictions of breakthrough curves for Phe.
Run nos. 3, 4

The models developed can be used directly for scale-up and can be extended to the prediction of the behavior of multicomponent systems.

Acknowledgment

This research was partially supported by National Science Foundation Grant No. CBT-8709011 and by Ajinomoto Co., Inc.

Notation

a = interfacial area per unit bed volume, cm^{-1}
c = macropore solute concentration, mol/L
C = liquid phase solute concentration, mol/L
$C_0 = C_{Cl^-} - C_{Na^+}$, mol/L
$C_{l,j}$ = equilibrium constant
D = macropore effective diffusivity, cm^2/s
$\bar{D}$ = microparticle effective diffusivity, cm^2/s
$E_{l,j}$ = adsorption energy for ion j on site l, J/mol
$\bar{E}_j$ = average adsorption energy of ion j, J/mol
J = flux through the macropore, $mol/cm^2 \cdot s$
$\bar{J}$ = flux through the microparticles, $mol/cm^2 \cdot s$
k_f = film mass transfer coefficient, cm/s
K_1 = dissociation equilibrium constant, mol/L
K_2 = dissociation equilibrium constant, mol/L
n = number of sites − 1

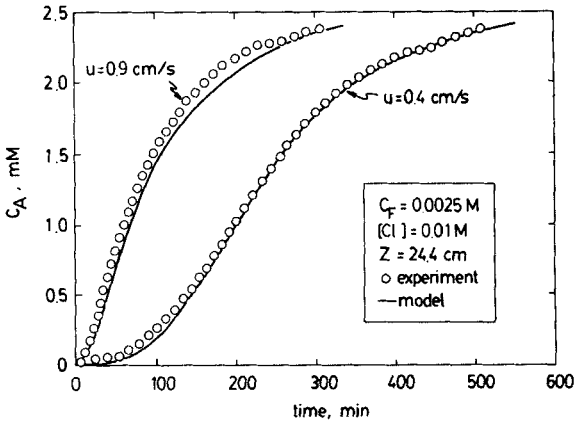

Figure 19. Experimental results and model predictions of breakthrough curves for Tyr.
Run nos. 5, 6

N = number of counterions or interior collocation points
NE = number of finite elements
$NT = N + 2$
NZ = number of interior collocation points in the z direction
p = skewness parameter, Eq. 16
p_l = probability distribution of site types l, Eq. 16
q = resin equilibrium uptake, mmol/g dry resin
q_o = resin ion-exchange capacity, mmol/g dry resin
q' = microparticle solute concentration, mol/L
q'_o = microparticle ion-exchange capacity, mol/L
$\bar{q}$ = resin average solute concentration, mmol/g dry resin
Q_L = liquid flow rate, cm^3/s
r = particle radial coordinate, cm
R = particle radius, cm
$S_{i,j}$ = separation factor for ion i relative to ion j, Eq. 21
$\bar{S}_{i,j}$ = average binary separation factor for ion i relative to ion j, Eq. 22
t = time, s
T = temperature
u = superficial velocity, cm/s
U = parameter, Eq. 24
V = parameter, Eq. 25
V_b = resin volume, cm^3
V_s = solution volume, cm^3
$W_{i,j}$ = heterogeneity parameter, Eq. 23
X = liquid phase ionic fraction
Y = resin phase ionic fraction
z = bed axial coordinate, cm
Z = bed length, cm

Greek letters

γ = variable, Eq. A7, cm^{-1}
ϵ = bed void fraction
ϵ_p = particle macroporosity
$\zeta = z/Z$
ξ = variable, Eq. A1
ρ_b = bed resin density, g dry resin/cm^3 of bed
ρ_p = particle resin density, g dry resin/cm^3 of particle
σ_j = standard deviation of energy distribution function for ion j, J/mol
ϕ = electrical potential, V

Superscripts

F = feed conditions
i = interfacial
o = initial conditions
calc = calculated value
exp = experimental value

Appendix A: Numerical Solution of Intraparticle Diffusion Model

A numerical solution of the intraparticle diffusion model, Eqs. 40–48, was obtained by orthogonal collocation on finite elements. This technique, originally introduced by Carey and Finlayson (1975) for diffusion problems, is capable of handling sharp concentration gradients that may occur near the particle surface, by combining the small truncation error of the orthogonal collocation method with the ability of the finite-difference method to locate the grid points where they are needed. Our solution was implemented as follows. As shown in Figure 20, the particle radius, R, is divided in an arbitrary number, NE, of finite elements of width Δr_l at r_l locations. Then, within each element l, N interior collocation points are chosen at the zeroes, ξ_l^i, of the Jacobi polynomials $P_N^{(\alpha,\beta)}(\xi_l)$ (Villadsen and Michelsen, 1978), where

$$\xi_l = \frac{r - r_l}{\Delta r_l} \tag{A1}$$

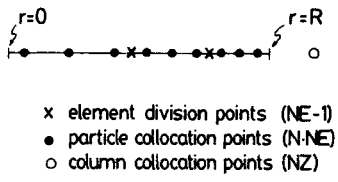

Figure 20. Layout of finite elements and collocation points for numerical solution of intraparticle transport equations.

α and β were set equal to zero. Dropping the subscript A, the intraparticle solute concentration and its derivatives at the interior collocation points may be expressed as

$$c(\xi_l^i, t) = \sum_{k=1}^{NT} l_k(\xi_l^i) c(\xi_l^k, t) \tag{A2}$$

$$\frac{\partial c(\xi_l^i, t)}{\partial r} = \frac{1}{\Delta r_l} \sum_{k=1}^{NT} l_k^{(1)}(\xi_l^i) c(\xi_l^k, t) \tag{A3}$$

$$\frac{\partial^2 c(\xi_l^i, t)}{\partial r^2} = \frac{1}{(\Delta r_l)^2} \sum_{k=1}^{NT} l_k^{(2)}(\xi_l^i) c(\xi_l^k, t) \tag{A4}$$

where $NT = N + 2$, and l_k, $l_k^{(1)}$ and $l_k^{(2)}$ are the interpolation weights of Lagrange interpolation polynomials. Equations A2–A4 are used to discretize Eq. 40 in the radial direction, yielding a system of $NE \times N$ ODE's at the interior collocation points. At $r = 0$ and $r = R$, boundary conditions 44 and 46 yield, respectively,

$$\sum_{k=1}^{NT} l_k^{(1)}(\xi_1^1) c(\xi_1^k, t) = 0 \tag{A5}$$

and

$$\frac{1}{\Delta r_{NE}} \sum_{k=1}^{NT} l_k^{(1)}(\xi_{NE}^1) c(\xi_{NE}^k, t) = \gamma(\xi_{NE}^{NT}, t)[C_A(t) - c(\xi_{NE}^{NT}, t)] \tag{A6}$$

where

$$\gamma(r, t) = \frac{k_f}{\epsilon_p D_A + (1 - \epsilon_p)\bar{D}_A \partial q'_A / \partial c_A} \tag{A7}$$

Continuity of the function and of its first derivative is required at the $NE - 1$ element division points, yielding

$$c(\xi_l^{NT}, t) = c(\xi_{l+1}^1, t) \tag{A8}$$

$$\frac{1}{\Delta r_l} \sum_{k=1}^{NT} l_k^{(1)}(\xi_l^{NT}) c(\xi_l^k, t) = \frac{1}{\Delta r_{l+1}} \sum_{k=1}^{NT} l_k^{(1)}(\xi_{l+1}^1) c(\xi_{l+1}^k, t) \tag{A9}$$

Equations A5–A9 can be rearranged to form the following tridiagonal system of algebraic equations that allows the computation of the values of c at the element division points, when the c values are known at the interior collocation points. For the first element ($l = 1$) one has

$$l_1^{(1)}(\xi_1^1) c(\xi_1^1, t) + l_{NT}^{(1)}(\xi_1^{NT}) c(\xi_1^{NT}, t) = \sum_{k=2}^{N+1} l_k^{(1)}(\xi_1^1) c(\xi_1^k, t) \tag{A10}$$

for the interior elements ($l = 2, 3, \ldots, NE - 2$)

$$\frac{l_1^{(1)}(\xi_l^{NT})}{\Delta r_l} c(\xi_l^{NT}, t) + \left[\frac{l_{NT}^{(1)}(\xi_l^{NT})}{\Delta r_l} - \frac{l_1^{(1)}(\xi_{l+1}^1)}{\Delta r_{l+1}}\right] c(\xi_l^{NT}, t) - \frac{l_{NT}^{(1)}(\xi_{l+1}^1)}{\Delta r_{l+1}} c(\xi_{l+1}^{NT}, t) = \frac{1}{\Delta r_{l+1}} \cdot \sum_{k=2}^{N+1} l_k^{(1)}(\xi_{l+1}^1) c(\xi_{l+1}^k, t) - \frac{1}{\Delta r_l} \sum_{k=2}^{N+1} l_k^{(1)}(\xi_l^{NT}) c(\xi_l^k, t) \quad \text{(A11)}$$

and for the last element ($l = NE - 1$)

$$\frac{l_1^{(1)}(\xi_{NE}^{NT})}{\Delta r_{NE}} c(\xi_{NE}^1, t) + \left[\frac{l_{NT}^{(1)}(\xi_{NE}^{NT})}{\Delta r_{NE}} + \gamma\right] c(\xi_{NE}^{NT}, t) = \gamma C(t) - \frac{1}{\Delta r_{NE}} \sum_{k=2}^{N+1} l_k^{(1)}(\xi_{NE}^{NT}) c(\xi_{NE}^k, t) \quad \text{(A12)}$$

The numerical algorithm was implemented using subroutine DFOPR, given by Villadsen and Michelsen (1978) to compute the interpolation weights. The system of $NE \times N$ ODE's, coupled with Eqs. A10–A12 and the material balance for the bulk fluid, were integrated using subroutine DGEAR in the IMSL library. Ordinarily, three interior collocation points and seven elements spaced at $r/R = 0, 0.05, 0.3, 0.6, 0.8, 0.9, 0.95$, and 1 were used for the calculation. The accuracy of the numerical algorithm was tested by comparing the results of the numerical solution to the available analytic solution for linear adsorption from a finite bath (Ruthven, 1984).

Finally, it should be noted that it is also possible to avoid having to solve the system of algebraic equations at each time step, by using cubic Hermite polynomials, which automatically insure continuity at the element boundaries (Costa and Rodrigues, 1985). Such polynomials yield, however, an implicit system of ODE's. Using Jacobi polynomials, as we have done, yields explicit ODE's and a tridiagonal system of algebraic equations, which can be solved rather efficiently with the Thomas algorithm.

Appendix B: Numerical Solution of Fixed-Bed Model

For the solution of the fixed-bed model equations, since sharp concentration gradients in the bed axial direction are not expected (if they are, a moving finite-element scheme may be implemented), regular collocation is used. The differential mass balance for the fixed bed, Eq. 49, is discretized in the axial coordinate of the bed by collocation at the NZ roots, ζ_j, of Jacobi polynomials $P_{NZ}^{(\alpha,\beta)}(\zeta)$, yielding

$$\epsilon \frac{dC(\zeta_j, t)}{dt} = -k_f a\,[C(\zeta_j, t) - c(\zeta_j, \xi_{NE}^{NT}, t)] - \frac{u}{Z} \sum_{k=1}^{NZ+2} l_k^{(1)}(\zeta_j) C(\zeta_k, t) \quad \text{(B1)}$$

at the $NZ + 2$ collocation points. Values of α and β equal to zero were again used. The $NZ + 2$ ODE's are solved simultaneously with the particle diffusion equations, discretized as described in Appendix A. Typically, six to eight internal collocation points were used along the axial coordinate to compute breakthrough and elution curves. The numerical solution was again tested for accuracy by comparison with the Anzelius solution (Ruthven, 1984) and with available constant-pattern solutions for Langmuir isotherms.

Literature Cited

Barrer, R. M., and W. M. Meier, "Exchange Equilibrium in a Synthetic Crystalline Exchanger," *Trans. Faraday Soc.*, **55**, 130 (1959).

Blackburn, S., "Amino Acids and Amines," *Handbook of Chromatography*, G. Zweig, J. Sherma, eds., CRC Press, Boca Raton, Fl, 1983.

Campbell, R. J., Jr., "Ion Exchange of Tyrosine on a Cationic Resin: Equilibrium and Mass Transfer Characteristics," M.S. Thesis, Univ. Virginia, Charlottesville (1987).

Carey, G. F., and B. A. Finlayson, "Orthogonal Collocation on Finite Elements," *Chem. Eng. Sci.*, **30**, 587 (1975).

Costa, C., and A. E. Rodrigues, "Design of Cyclic Fixed-Bed Adsorption Processes," *AIChE J.*, **31**, 1645 (Oct., 1985).

Feitelson, J., "Interactions of Dipolar Ions with Ionized Polymers. Electrostaic and Specific Effects," *J. Phys. Chem.*, **65**, 975 (1961).

———, "Specific Effects in the Interaction between Ion-Exchange Resins and Amino Acid Cations," *J. Phys. Chem.*, **67**, 2544 (1963).

Hamilton, P. B., D. C. Bogue, and R. A. Anderson, "Ion-Exchange Chromatography of Amino Acids," *Anal. Chem.*, **32**, 1782 (1960).

Helfferich, F., *Ion Exchange*, McGraw-Hill, New York (1962).

———, "Ion-Exchange Kinetics. V: Ion Exchange Accompanied by Reactions," *J. Phys. Chem.*, **11**, 1178 (1965).

Kataoka, T., H. Yoshida, and T. Yamada, "Liquid Phase Mass Transfer in Ion Exchange Based on the Hydraulic Radius Model," *J. Chem. Eng. Japan*, **6**, 172 (1973).

Kataoka, T., H. Yoshida, and H. Sanada, *J. Chem. Eng. Japan*, **7**, 105 (1974).

Myers, A. L., and S. Byington, "Thermodynamics of Ion Exchange: Prediction of Multicomponent Equilibria from Binary Data," *Ion Exchange Science and Technology*, A. E. Rodrigues, ed., NATO ASI, Series E., No. 107, Nijhoff, Dordrecht (1986).

Novosad, J., and A. L. Myers, "Thermodynamics of Ion Exchange as an Adsorption Process," *Can. J. Chem. Eng.*, **60**, 500 (1982).

Patell, S., and J. C. R. Turner, "The Equilibrium and Sorption Properties of Some Porous Ion Exchangers," *J. Sep. Proc. Technol.*, **1**, 42 (1979).

———, "The Kinetics of Ion Exchange Using Porous Exchangers," *J. Sep. Proc. Technol.*, **1**, 31 (1980).

Reichenberg, D., and D. J. McCauley, "Properties of Ion-Exchange Resins in Relation to their Structure. VII: Cation Exchange Equilibrium on Sulfonated Polystyrene Resins of Varying Degree of Crosslinking," *J. Chem. Soc.*, 2741 (1955).

Ruthven, D. M., *Principles of Adsorption and Adsorption Processes*, Wiley, New York (1984).

Seno, M., and T. Yamabe, "The Ion-Exchange Behavior of Some Neutral Amino Acids," *Bull. Chem. Soc. Japan*, **33**, 1532 (1960).

———, "Ion Exchange of Acidic and Basic Amino Acids," *Bull. Chem. Soc. Japan*, **34**, 102 (1961).

Soldatov, V. S., and V. A. Bichkova, "Ion-Exchange Selectivity and Activity Coefficients as Functions of Ion-Exchange Composition," *Ion Exchange Technology*, D. Naden, M. Streat, eds., Horwood, Chichester (1984).

Turner, J. C. R., M. R. Church, A. S. W. Johnson, and C. B. Snowdon, "An Experimental Verification of the Nernst-Planck Model for Diffusion in Ion-Exchange Resins," *Chem. Eng. Sci.*, **21**, 317 (1966).

Villadsen, J., and M. L. Michelsen, *Solution of Partial Differential Equation Models by Polynomial Approximation*, Prentice-Hall, Englewood Cliffs, NJ (1978).

Yamada, K., S. Kinoshita, T. Tsunoda, and K. Aido, *The Microbial Production of Amino Acids*, Halsted, Wiley, New York (1972).

Yoshida, H., T. Kataoka, and S. Ikeda, "Intraparticle Mass Transfer in Bidisperse Porous Ion Exchangers. I: Isotopic Ion Exchange," *Can. J. Chem. Eng.*, **63**, 422 (1985).

Yoshida, H., and T. Kataoka, "Intraparticle Mass Transfer in Bidisperse Porous Ion Exchangers. II: Mutual Ion Exchange," *Can. J. Chem. Eng.*, **63**, 430 (1985).

Yu, Q., and N.-H.L. Wang, "Multicomponent Interference Phenomena in Ion-Exchange Columns," *Sep. Purif. Meth.*, **15**, 127 (1986).

Yu, Q., J. Yang, and N.-H.L. Wang, "Multicomponent Ion-Exchange Chromatography for Separating Amino Acid Mixtures," *React. Polym.*, **6**, 33, (1987).

Manuscript received May 19, 1988, and revision received Sept. 26, 1988.